# Boundary lubrication with a liquid crystal monolayer

W. Chen,[1,*] S. Kulju,[2] A. S. Foster,[1] M. J. Alava,[1] and L. Laurson[1]

[1]*COMP Centre of Excellence, Department of Applied Physics, Aalto University, P.O. Box 11100, FI-00076 AALTO, Espoo, Finland*

[2]*Department of Physics, Tampere University of Technology, P.O. Box 692, FI-33010 Tampere, Finland*

(Received 17 April 2014; published 23 July 2014)

We study boundary lubrication characteristics of a liquid crystal (LC) monolayer sheared between two crystalline surfaces by nonequilibrium molecular dynamics simulations, using a simplified rigid bead-necklace model of the LC molecules. We consider LC monolayers confined by surfaces with three different atomic structures, subject to different shearing velocities, thus approximating a wide variety of materials and driving conditions. The time dependence of the friction force is studied and correlated with that of the orientational order exhibited by the LC molecules, arising from the competition between the effect of the structure of the confining surfaces and that of the imposed sliding direction. We show that the observed stick-slip events for low shear rates involve order-disorder transitions, and that the LC monolayer no longer has enough time to reorder at high shear rates, resulting in a smooth sliding regime. An irregular stick-slip phase between the regular stick-slip and smooth sliding is observed for intermediate shear rates regardless of the surface structure.

DOI: 10.1103/PhysRevE.90.012404 PACS number(s): 81.40.Pq, 83.80.Xz

## I. INTRODUCTION

Understanding the processes at the interface of two solid surfaces in contact and in relative sliding motion is central to many technological applications, and involves open questions of the nature of fundamental physics even today, ranging from the atomistic and nanoscale [1] to macroscopic systems [2]. From the practical point of view, using lubricant layers separating the two solid surfaces helps in reducing friction and wear, thus significantly increasing the energy efficiency and service life of mechanical devices [3]. In order to speed up the development process of new lubricants with optimized frictional properties, an improved understanding of the general topic of physics of confined systems under shear is needed. Often the relevant phenomena and processes are intimately related to fundamental properties of such systems, e.g., to the phase behavior of the lubricant layer, or to closely related systems such as unconfined adsorbed molecularly thin films sliding on substrates [4].

The idea of using monomer liquid crystal (LC) molecules [5] as lubricants or lubricant additives dates back almost 30 years [6], and has more recently been shown to produce a dramatic reduction of friction to ultralow values [7–10]. Recent studies have also focused on tailored LC lubricants, with emphasis on balancing efficiency with effective cost [11]. In order to make further progress in the optimization of frictional properties of LC lubricants, a thorough understanding of the structural and dynamical properties of LC molecules under shear conditions is critical. So far, the mechanisms of the ultralow friction coefficients are not fully clear, but several studies indicate that external pressure and shear stress can induce a molecular ordering of the LC molecules [12–14]. A theoretical explanation of the dependence of the friction force on the molecular orientation has also been proposed [15], indicating that an increase in the shear velocity results in an alignment of the LC molecules with the flow, and consequently in a reduction of the friction force. Such connections between the friction force and the molecular orientation have also been observed in surface force apparatus experiments on 8CB LCs confined by mica surfaces, where, e.g., an anisotropic critical shear stress has been observed [16]. Moreover, transitions between smooth and complex stick-slip sliding of branched hydrocarbons which can exhibit a liquid crystalline state under confinement have been observed [17]. Nevertheless, the effect of the details of the complex interplay of the structure of the confining surfaces, that of the confined LCs, and the imposed sliding velocity on the frictional response of the system remain to be fully understood, within the boundary lubrication (monolayer) regime in particular.

One of the principal tools in the study of fluids is molecular dynamics (MD) simulations [18]. Indeed, numerous equilibrium and nonequilibrium MD simulation studies of flow phenomena in bulk LC systems have been performed [19–24]. However, simulations of confined LC molecules subject to shear are less common: Simplified models of the Gay-Berne type have been considered [25,26], but, in general, to our knowledge, extensive numerical studies of LC lubricants have not been performed. Here we consider the key structural and dynamical properties of confined LC molecules under shear conditions by performing nonequilibrium MD simulations of a simplified rigid bead-necklace model of the LC molecules [27–29], confined by sliding surfaces with three different atomic structures. Previous simulations of similar models for flexible polymers have shown that the bead-necklace models capture much of the structural and dynamic properties of confined polymer fluids undergoing flow [30,31], and thus we expect the model, despite its simplicity, to capture the main features of the problem of LC lubrication as well. We focus on the boundary lubrication regime, where the sliding surfaces are separated by a LC monolayer. We note that Drummond and Israelachvili have performed experiments using a somewhat similar setup, i.e., two sliding mica surfaces confining a thin film of branched hydrocarbons [32,33]. There, regular stick-slip, "chaotic," or irregular stick-slip and smooth sliding states were observed using a surface force apparatus, similarly to theoretical results obtained for ultrathin liquid films confined

*wei.chen@aalto.fi

 

by atomically flat surfaces [34]. In our simulations, we determine the friction force of the confined LC monolayer under different shearing and sliding conditions by considering three different atomic structures for the confining surfaces. We find similar transitions from stick-slip to smooth sliding via an irregular stick-slip state as the imposed sliding velocity is increased. We investigate the connection between the observed frictional response and the ordering characteristics of the LC monolayer. In particular, we show that depending on the atomic structure of the confining surfaces, the stick-slip events observed for low shear rates may involve order-disorder transitions of the LC monolayer, and that the monolayer no longer has enough time to reorder at high enough shear rates, resulting in a smooth sliding regime. The paper is organized as follows: The details of the simplified model system and the nonequilibrium MD simulations are described in Sec. II. The simulation results are presented in Sec. III. A summary of the results and conclusions are given in the final Sec. IV.

## II. MODEL

We consider a coarse-grained rigid bead-necklace model [27–29], shown schematically in the top panel of Fig. 1. The beads belonging to different molecules interact according to the Lennard-Jones 12-6 potential,

$$U_{ij} = 4\epsilon\left[\left(\frac{\sigma}{r_{ij}}\right)^{12} - \left(\frac{\sigma}{r_{ij}}\right)^{6}\right], \qquad (1)$$

where $U_{ij}$ is the interaction potential for beads $i$ and $j$ separated by a distance $r_{ij}$. Without loss of generality, all quantities are reported in reduced units. The temperature, pressure, and time are defined, respectively, as [35] $T^* = Tk_B/\epsilon$, $P^* = P\sigma^3/\epsilon$, and $\tau = t^* = t\sqrt{\epsilon/m\sigma^2}$, and the fundamental quantities $\sigma$, $\epsilon$, and the Boltzmann constant $k_B$ are set equal

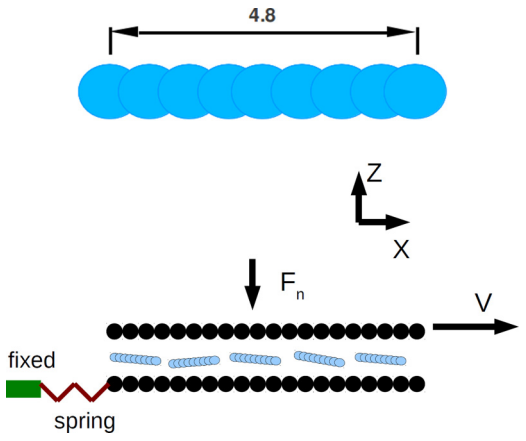


FIG. 1. (Color online) Top: Sketch of the rigid bead-necklace molecule, consisting of nine uniformly spaced interaction sites (beads) with the total length of the molecule equal to 4.8 in the reduced units considered here (see text). Bottom: The geometry of the simulation system, with the $y$ axis normal to the page. Blue molecules are the LC mesogens, confined by two crystalline plates (black beads) to form a monolayer. The bottom plate is connected to a fixed point by a spring, while the top plate is subject to a normal force $F_n$, and is moving with a constant velocity $V$ along the $x$ direction.

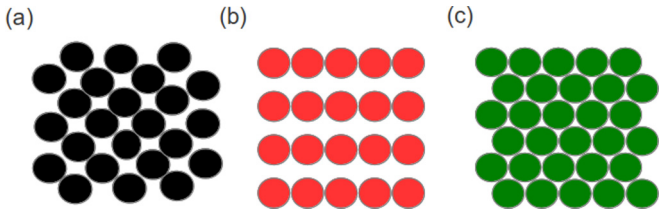


FIG. 2. (Color online) Atomic structure of the three confining surfaces considered. (a) (100) surface. (b) (110) surface. (c) (111) surface.

to one. Each LC molecule consists of nine interaction sites or beads of mass $m = 1.0$, the centers of which are separated by a distance of 0.6. The cutoff radius for the interaction is $r_c = 2.5$, and the total number of LC molecules is $N = 192$, which is fixed throughout all of the MD simulations considered.

The bottom panel of Fig. 1 shows a sketch of the simulation geometry. The LC molecules are confined by two rigid crystalline plates. For simplicity, each molecular bead interacts with the plate atoms via the same potential as for the intermolecular interaction, i.e., Eq. (1), with the same $\sigma$, $\epsilon$, and $r_c$. To account for the effects due to the structure of the confining surfaces on friction, three different surface structures are considered, shown in Fig. 2. The (100) surface is obtained by cutting the face-centered cubic (fcc) unit cell at position $\mathbf{a} = 1$, parallel to the $\mathbf{b}$ and $\mathbf{c}$ axes. The (110) surface is obtained by cutting the fcc unit cell at $\mathbf{a} = 1$ and $\mathbf{b} = 1$, parallel to the $\mathbf{c}$ axis. Similarly, the (111) plane is obtained by cutting the fcc metal in such a way that the surface plane intersects the $\mathbf{a}$, $\mathbf{b}$, and $\mathbf{c}$ axes at the same value, while the edge length of a cubic unit cell is fixed to unity. Each surface has a single layer of atoms. We have checked that the results do not change significantly if thicker confining surfaces are considered: the larger inertial mass of the thicker surfaces as well as the small additional interactions due to the atomic layers beyond the first one lead to small changes in the period and amplitude of the stick-slip oscillations, but otherwise the monolayer surfaces are representative of the more general case of thicker confining surfaces. The top surface always has the same structure as the bottom one. We use periodic boundary conditions in both the $x$ and $y$ directions. The simulation box dimensions in the $xy$ plane are chosen to be $L_x = 48.0$ and $L_y = 36.0$. The number of the atoms in each surface $N_p$ is 6912 for the (100) surface, 4824 for the (110) surface, and 7956 for the (111) surface. The bottom plate is only allowed to move along the $x$ axis, and is attached to a spring of stiffness $K/N_p = 0.005$. We have checked that other $K$ values do not change the physics of the system, and affect mainly the period of the stick-slip oscillations, with stiffer springs leading to shorter stick-slip periods. The regions of the parameter space where one obtains the different dynamical regimes (stick-slip, smooth sliding) could also be affected by $K$. However, this effect was found to be weak, and thus difficult to characterize in detail. One end of the spring connects to a stage which is kept fixed during the simulations. The system is driven by moving the top plate at a constant velocity $V$ along the positive $x$ direction. The top plate is allowed to move vertically and is subject to a constant normal load, $F_n/N_p = -1.0$. This normal load ensures that the confined LCs exhibit a monolayer

structure: In our simulations, the vertical distance $h$ between the two parallel plates is always less than 3.0 in the reduced units defined above, and the relative fluctuations $\delta h/\langle h\rangle$ are very small. Thus, the confined lubricant layer can be well described as a quasi-two-dimensional system.

It is important to note that the total velocity of a particle is the sum of its streaming velocity due to the imposed shear and its thermal velocity—the latter is what is needed to compute the temperature [36]. Hence, the thermostatting should subtract out the streaming bias and only act on the remaining thermal velocity. In this work, a Langevin thermostat is applied only in the $y$ direction, which is a common thermostatting procedure used in MD simulations of confined sheared fluids [31,37,38]. In this case, the equations of motion of the $i$th bead are

$$m\frac{dv_{i,x}(t)}{dt} = F_{i,x}(t), \tag{2}$$

$$m\frac{dv_{i,y}(t)}{dt} = F_{i,y}(t) - m\eta v_{i,y}(t) + f_i(t), \tag{3}$$

$$m\frac{dv_{i,z}(t)}{dt} = F_{i,z}(t), \tag{4}$$

where $\mathbf{v}_i = (v_{i,x}, v_{i,y}, v_{i,z})$ is the bead velocity and $\mathbf{F}_i = (F_{i,x}, F_{i,y}, F_{i,z})$ is the net deterministic force acting on the $i$th bead. $f_i(t)$ is a $\delta$-correlated stationary Gaussian process with zero mean, satisfying $\langle f_i(t)\rangle = 0$ and $\langle f_i(t) f_j(t')\rangle = 2mk_BT\eta\delta(t-t')\delta_{ij}$. $\eta$ is the damping factor which is equal to 0.01 in our simulations. The temperature of the thermostat is fixed at $T^* = 1.1$ for all simulations. The rigid bead-necklace molecular structure is maintained during the simulation by the methods described in the paper of Miller *et al.* [39].

The equations of motion are solved with the velocity Verlet algorithm as implemented in the Large-scale Atomic/Molecular Massively Parallel Simulator (LAMMPS) [40], with an integration time step of $0.001\tau$. The MD simulations were performed by the following procedure: In the initial state, the LC molecules are in the solid phase, with the long axes of each molecule parallel to the $x$ axis. All simulations are first run for a total of $10^5$ time steps while the vertical distance between the surfaces is kept at 10.0 and both plates are kept fixed. After that, the normal force is applied to the top plate and is allowed to move vertically for a period of $10^5$ time steps. Then, the bottom plate is allowed to move and the top plate is driven horizontally with the target velocity for $10^6$ time steps to generate the steady state. Once the steady state is reached, typical production runs of a total of $10^6$ ($10^3\tau$) time steps are run with averages accumulated in every 100 time steps. The orientational order parameters of the LC molecules are determined by postprocessing of the dump files from LAMMPS [41].

## III. RESULTS

MD simulation results for LC molecules confined by different kinds of surfaces under different driving velocities of the top plate are shown in Fig. 3. The maximum driving velocity in our simulations is $V = 0.5$, which is 50 times larger

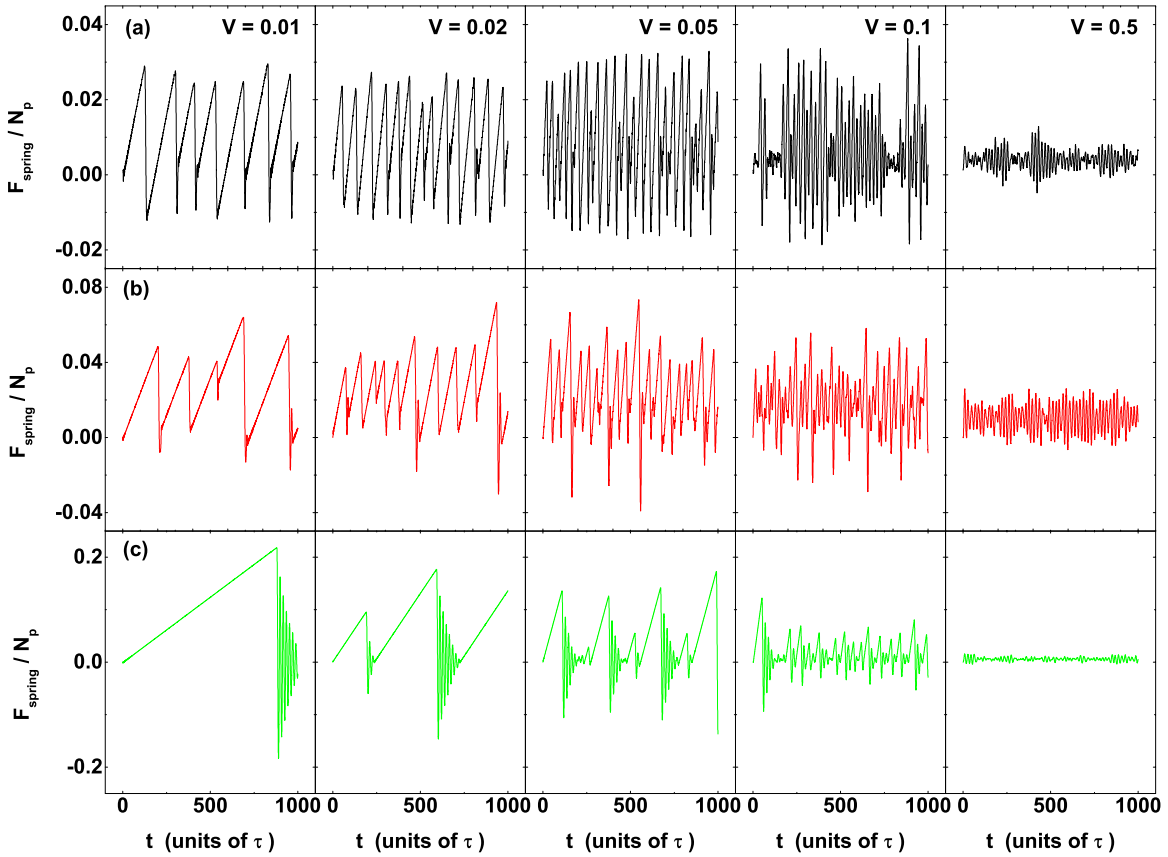


FIG. 3. (Color online) The spring forces obtained at different driving velocities for LC molecules confined by (a) (100) surfaces, (b) (110) surfaces, and (c) (111) surfaces.

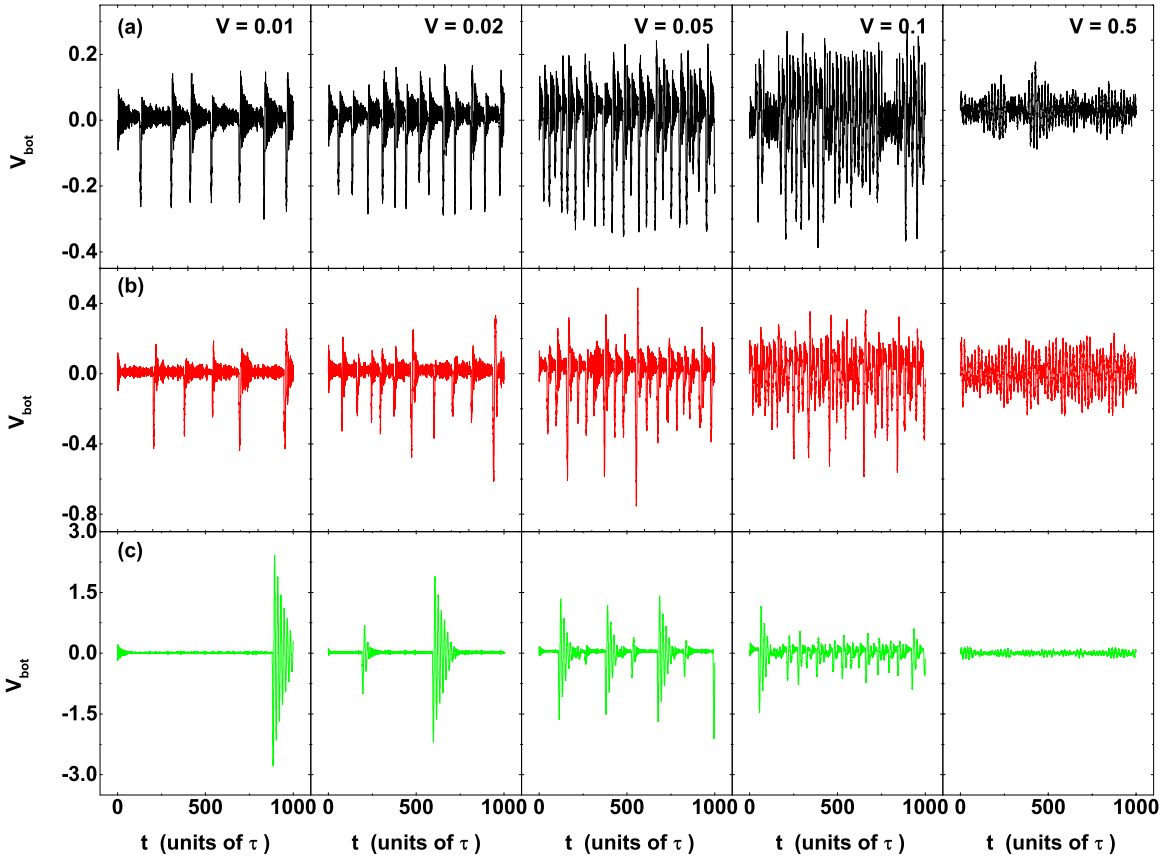


FIG. 4. (Color online) The velocities of the bottom plate at different driving velocities for LC molecules confined by (a) (100) surfaces, (b) (110) surfaces, and (c) (111) surfaces.

than the minimum one, $V = 0.01$. Our results are similar to experiments on thin films of branched hydrocarbons [32,33]: Figure 3 shows that at low sliding velocities, the system exhibits highly regular stick-slip events for all three kinds of surfaces. Initially, the bottom plate is in a stick state. The force per plate atom applied by the spring $F_{\text{spring}}/N_p$ then increases linearly, eventually exceeding the maximum static friction force (the force needed to initiate sliding), and the bottom plate begins to slip. Since the kinetic friction force is smaller than the static one, the bottom plate accelerates to jump back, and the force applied by the spring decreases. Then the bottom plate sticks once again, and the process repeats. As the smooth sliding phase is approached by increasing the driving velocity, the maximum value of $F_{\text{spring}}/N_p$ is much smaller than that of stick-slip events. The stick-slip and smooth sliding phases are separated by an irregular stick-slip phase: the bottom plate oscillates irregularly with different amplitudes. Similar results have also been observed before in simulations of simple spherical molecules [42,43].

The forces applied by the spring have roughly the same order of magnitude for the LC molecules confined by the (100) and (110) surfaces, and experience similar trends with the sliding velocity. However, the maximum measured force for LC molecules confined by the (111) surface, as shown in Fig. 3(c), is about one order of magnitude larger, and the frequency of the stick-slip cycle is much smaller at the same driving velocity: There is only one cycle for the velocity $V = 0.01$ in the case of the (111) surface, while during the same time period, the (100) surface has seven cycles and the (110) surface has five. In addition, the bottom plate exhibits damped oscillations when it slips and, consequently, the LC molecules confined by the (111) surface need a much longer time (as compared to the other surface structures) to rearrange for the next stick state.

Figure 4 shows the time evolution of the velocity of the bottom place, $V_{\text{bot}}$, for the three different confining surfaces; the data correspond to that of the friction forces shown in Fig. 3. During one stick-slip cycle, for the (100) and (110) surfaces, $V_{\text{bot}}$ goes from almost zero (stick) to a minimum value (slip; this is negative since the bottom plate gets pulled back during the slip event) and back to zero again (stick). Similarly to what can be observed when looking at the friction forces in Fig. 3, regular stick-slip cycles can be distinguished clearly for low sliding velocities, while the period of cycles decreases as the driving velocity increases. When the period of the stick-slip cycle is close to the time needed for the LC molecules to fully rearrange, the bottom plate displays irregular, possibly chaotic behavior. At even higher driving velocities, the lubricant film no longer has time to rearrange and, consequently, a smooth sliding state is obtained. Notice again that the low-velocity stick-slip dynamics of the system with the (111) surface is different from that of the two other surfaces [Fig. 4(c)]: The maximum velocity of the bottom (111) plate at the onset of slip is one order of magnitude larger than those of the other two kinds of surfaces, and the plate exhibits damped oscillations.

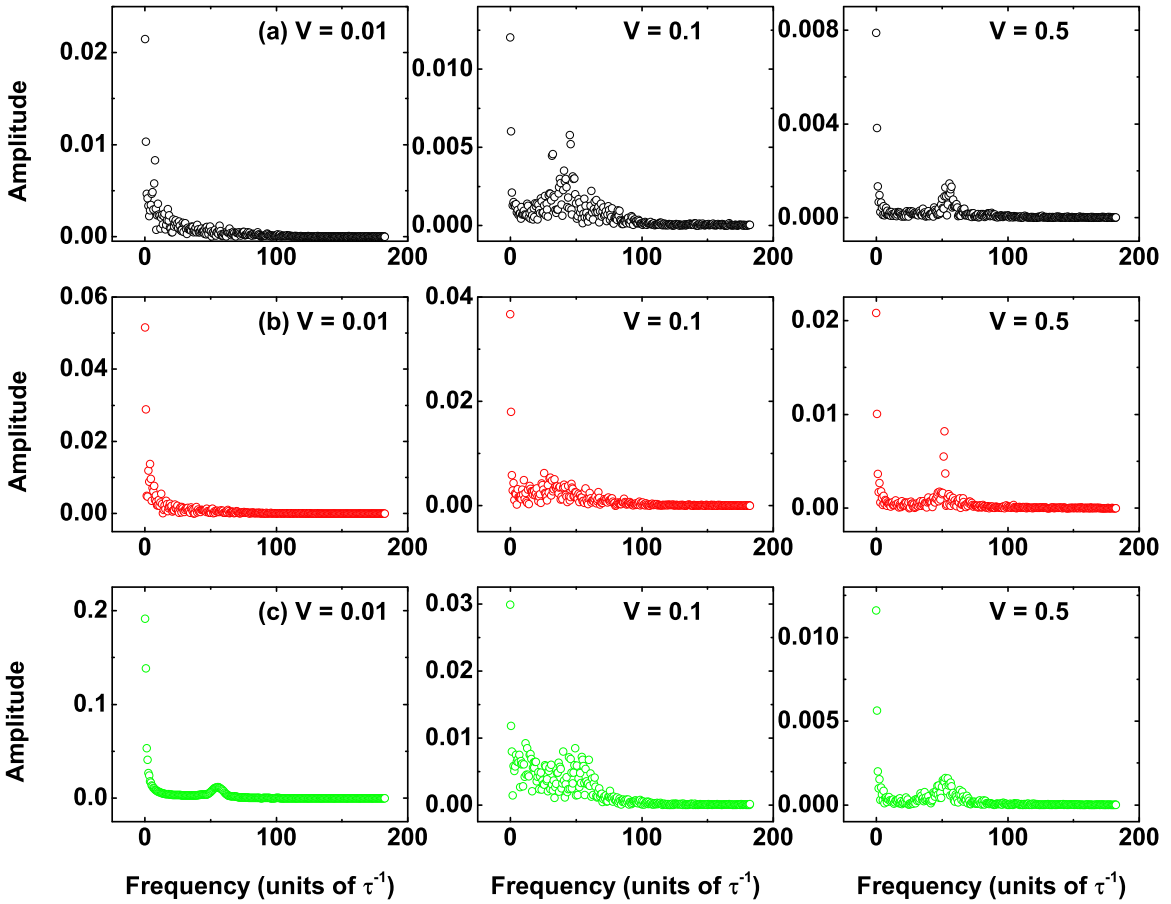


FIG. 5. (Color online) The Fourier transform of the spring forces at different driving velocities for LC molecules confined by (a) (100) surfaces, (b) (110) surfaces, and (c) (111) surfaces.

To further characterize the stick-slip dynamics, we consider the Fourier transform of the spring forces (like the ones shown in Fig. 3). Figure 5 shows the Fourier transform, i.e., the moduli of the complex amplitudes vs the frequency, of the force applied by the spring within the three phases, i.e., regular stick-slip, irregular stick-slip or chaos, and smooth sliding. At low driving velocities for the (100) and (110) surfaces, the stick-slip dynamics corresponds to a low-frequency sawtoothlike time evolution of the friction force, visible as a single low-frequency peak in the corresponding Fourier spectrum, shown in the left panels of Figs. 5(a) and 5(b). For the (111) surface, the damped oscillations show up as an additional higher-frequency peak [left panel of Fig. 5(c)]. For intermediate driving velocities corresponding to irregular stick-slip dynamics, the spectra in the middle panels of Fig. 5 show that more frequencies are present in the spring force time series, in particular in the form of a broad second peak emerging for intermediate and higher frequencies. The right panels of Fig. 5 display the spectra of the high-velocity smooth sliding states: There, it seems that the signal includes essentially two frequencies, i.e., a low-frequency component, as in the case of the low-velocity stick-slip phase, and an additional higher-frequency component.

To understand the mechanism of velocity dependence of the friction force, a broad range of parameters of the LC monolayer confined by the plates is studied for each kind of surface. The (111) surface has the most compact atomic arrangement and has a threefold symmetry (primitive surface mesh is a 60° rhombus) showing hexagonal packing. The snapshots [44] of instantaneous configurations of the LC film confined by the (111) surface for both the stick and the slip state at driving velocity $V = 0.01$ are shown in Fig. 6; a video file is provided in the Supplemental Material [45]. The LC molecules align their long axes roughly along the surface mesh in the stick state and include a number of domains with different local orientational order. When the bottom plate slips, the system

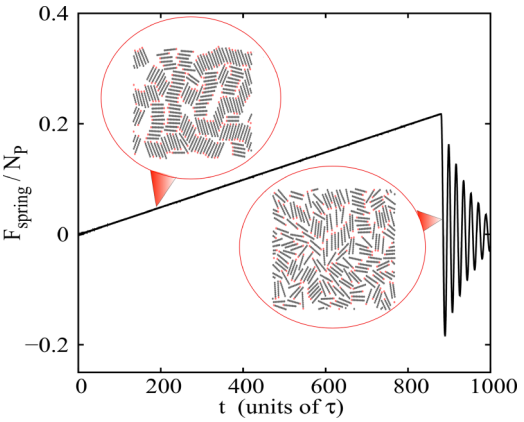


FIG. 6. (Color online) The snapshots of the LC monolayer confined by the (111) surfaces for the driving velocity of $V = 0.01$.

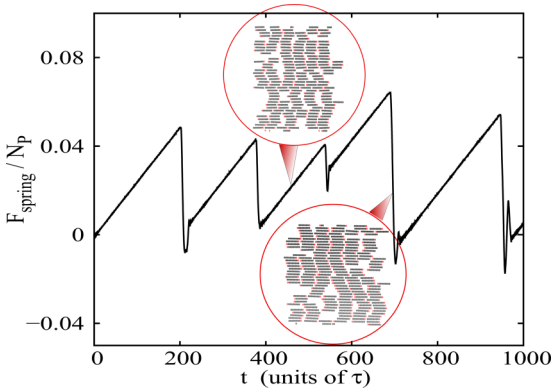


FIG. 7. (Color online) The snapshots of the LC monolayer confined by the (110) surfaces for the driving velocity of $V = 0.01$.

gets disordered: Thus, it will take some time for the LC molecules to rearrange themselves back to the more ordered stick state, which is something that may be related to the damped oscillations exhibited by the bottom plate with the (111) structure.

The atoms of the (110) surface are much less closely packed than those of the two other surfaces. The nearest atoms are arranged only in one direction, along the $x$ axis. Since the shear flow is also in this direction, the preferential orientation of the LC molecules does not change with the sliding speed (also the shear-induced orientation is along $x$). The snapshots of the instantaneous configurations of LC film confined by the (110) surface with a driving velocity of $V = 0.01$ are shown in Fig. 7: It is impossible to distinguish between the stick and slip states visually from such snapshots. Consequently, since no change in orientation of the LCs is needed, the system needs only a very short time to go from slip to stick, and thus no oscillations of the bottom plate are observed here (cf. Fig. 6).

Figure 8 shows snapshots of the corresponding configurations of the LC monolayer for the (100) surface (again, the $V = 0.01$ case is considered). The configurations are characterized by a high degree of order. The nearest plate atoms in the (100) surface are arranged along the 2D vectors

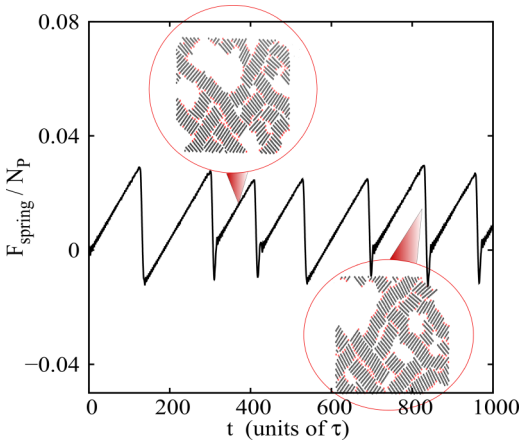


FIG. 8. (Color online) The snapshots of the LC monolayer confined by the (100) surfaces for the driving velocity $V = 0.01$.

in the $xy$ plane with the angles that equal $\pm 45^\circ$; thus the LC molecules tend to align with their long axes roughly along the angles of $\pm 45^\circ$. However, since there is no preferred direction along the sliding direction set by the confining surfaces, the molecules are aligned along the $\pm 45^\circ$ directions both in the stick and the slip states: Indeed, we cannot distinguish between the stick and slip states visually from Fig. 8. In both cases, we observe large domains with the molecules aligned along the $\pm 45^\circ$ directions, with some "empty pockets" in between, due to the combination of closely packed domain structures and the fact that we consider a fixed number of molecules confined by the plates. A somewhat different outcome could be expected if the simulations would be performed in a grand canonical ensemble, where the LC film would be in contact with an external reservoir [46].

In the stick state of the system with (111) surfaces, shown in Fig. 6, the LC monolayer consists of a number of domains within which the LC molecules are aligned, whereas this order is lost in the subsequent slip state. In order to further characterize the time evolution of such ordering of the LCs, we consider the probability $P$ to find two parallel LC molecules in the monolayer, and the average number of molecules in each domain, i.e., the average domain size. If the absolute value of the scalar product of two different LC molecules' unit vectors is greater than 0.985, i.e., the angle between the two unit vectors is less than $10^\circ$, these two LC molecules are considered to be parallel. In addition, if the distance between the centers of mass of two parallel molecules is less than the length of the molecule, they are taken to be in the same domain. As can be observed in Fig. 9, the probability $P$ is almost constant ($P \approx 0.3$–$0.4$) in the stick state, and drops to a value close to $P = 0.1$ in the slip state, consistent with the snapshots in Fig. 6. The time evolution of the domain size exhibits a similar trend: When the bottom plate sticks, the LC molecules are ordered into a small number of domains consisting of parallel molecules. When the static friction reaches its threshold,

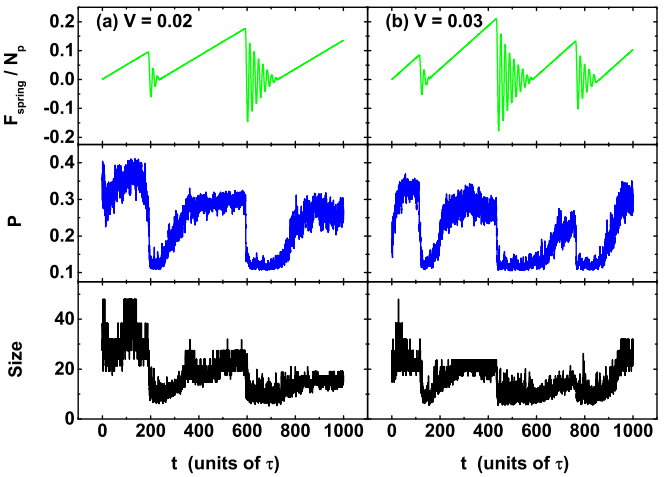


FIG. 9. (Color online) LC molecules confined by the (111) surfaces. The figures on the top row are the spring forces at different driving velocities: (a) $V = 0.02$, (b) $V = 0.03$. The figures in the middle row are the probabilities $P$ to find two parallel LC molecules. The figures on the bottom row show the time evolution of the average domain size.

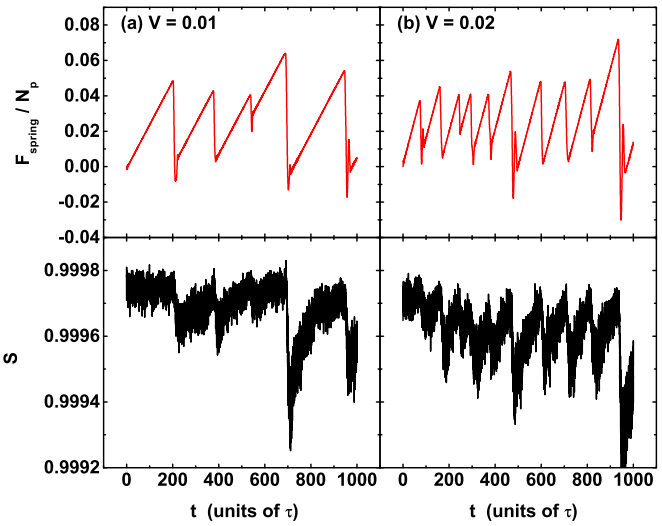


FIG. 10. (Color online) LC molecules confined by (110) surfaces, with (a) $V = 0.02$ and (b) $V = 0.03$. The figures in the top row display the spring forces, while those in the bottom row show the corresponding values of the order parameter $S$.

a rapid slip takes place, and such locally ordered domains disappear.

As for the (110) surface, the liquid crystals have a high degree of long-range orientation with their long axes always parallel. Thus the liquid crystals can be characterized in term of a global order parameter $S$, which is defined as the maximum eigenvalue of the average ordering tensor,

$$Q_{\alpha\beta} = \frac{1}{N}\sum_{i=1}^{N}\left(\frac{3}{2}u_\alpha^i u_\beta^i - \frac{1}{2}\delta_{\alpha\beta}\right), \tag{5}$$

where $u_\alpha^i$ $(\alpha,\beta = x,y,z)$ is the Cartesian component of the unit vector of the LC molecule $i$, and the sum is over the $N$ liquid crystal molecules. Examples of the order parameter $S$ as a function of time for two different low driving velocities are shown in Fig. 10. The order parameter reaches a value close to 1.0, which is expected since the sliding surfaces are separated by a very thin film, with all of the molecules in the monolayer strongly influenced by the surface mesh, resulting in a highly ordered configuration (see Fig. 7). However, the small but clearly observable fluctuations visible in the time evolution of $S$ indicate that small rearrangements of the LC molecules take place: a small drop of the $S$ value is observed whenever a slip event occurs.

We do not observe similar behavior for the (100) surface. In this case, there are many domains with local order in the LC film confined by the (100) surface, so the global order parameter $S$ defined in Eq. (5) is not able to measure the degree of general order in the film. Since the (100) surface has simply a square primitive surface mesh, there are two preferred directions for the LC molecules, but the (111) surface has three preferred directions (primitive surface mesh is a 60° rhombus). It is easier to form two parallel LC molecules on the (100) surface, and the time interval for the LC film to rearrange is ultrashort (a video file is provided in the Supplemental Material) [45]. Thus, there is no way to clearly distinguish between the stick and slip states by looking at quantities related to the orientational order of the LC monolayer confined by the (100) surfaces.

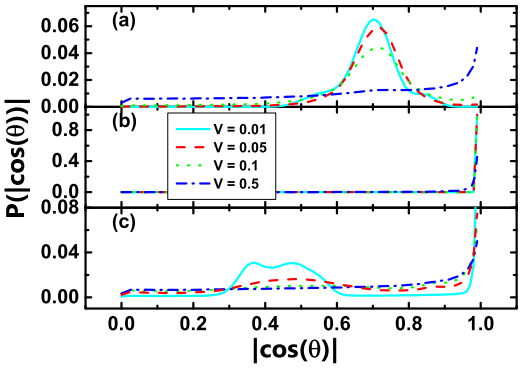


FIG. 11. (Color online) The distribution of $|\cos(\theta)|$ for LC molecules confined by (a) the (100) surfaces, (b) the (110) surfaces, and (c) the (111) surfaces.

The maximum friction force in the smooth sliding cases is much smaller than in the low-velocity stick-slip phases. Since the LC molecules may be able to reduce the friction by orienting themselves on the confining surfaces [11], one could expect the orientation of the LCs to depend on the driving velocity. In order to quantify this hypothesis, we examined the distribution of $|\cos(\theta)|$, where $\theta$ is the angle between the $x$ axis and the unit vector of the LC molecule. The distributions of $|\cos(\theta)|$ for the LC monolayer confined by (100) surfaces sliding at different velocities are plotted in Fig. 11(a). For low driving velocities, the liquid crystals align themselves along the surface mesh, with the most frequently occurring angle $\theta$ at around $\pm 45°$. The fraction of LC molecules with $\theta = \pm 45°$ decreases with increasing driving velocity, and the liquid crystals eventually become preferentially aligned in the direction of the shear flow ($\theta = 0$). In contrast, the alignment direction of the LCs confined by the (110) surfaces [Fig. 11(b)] is the same as the shear flow direction, irrespective of the sliding velocity. This is due to the fact that in that case, the preferred orientations induced by the surface structure and that due to the sliding direction coincide: Consequently, $|\cos(\theta)|$ is close to 1.0 at any driving velocity. Figure 11(c) shows the corresponding distributions for LC molecules confined by the (111) surface: The LCs align with their long axes roughly along the surface mesh (i.e., around $\pm 60°$) for the lowest driving velocity, and exhibit again a similar evolution of the preferred orientation to be along the shear flow when the sliding velocity is increased.

Boundary lubrication occurs when the sliding surfaces are separated by a thin lubricant film. In our simulations, the distance between the surfaces is no more than 3.0 in the reduced units; thus, all LC molecules in the monolayer can be considered to lie in the $xy$ plane. To study the velocity-dependent behavior of the LC spatial organization in the plane, we compute a plane pair distribution function $\rho(r)$, which is defined as an average of the number of molecular centers of mass lying within the range $r$ to $r + dr$ from a reference LC molecule, with the pair parallel to each other (according to the same definition as above, i.e., within an angle of 10°). Here, we only need the components of the coordinates within the

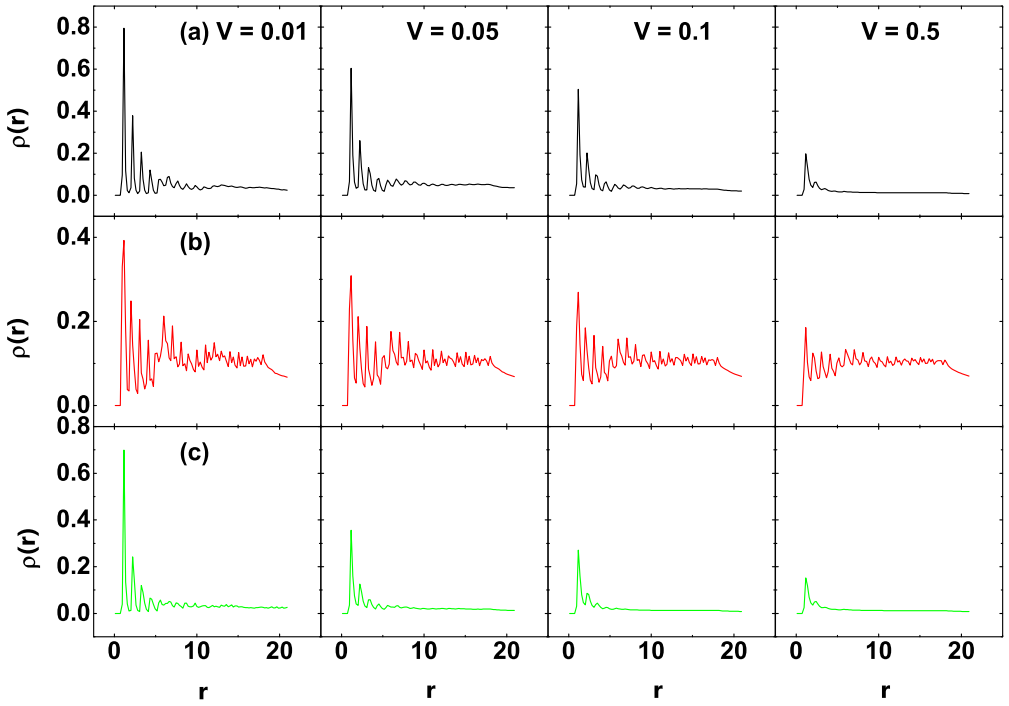


FIG. 12. (Color online) The planar pair distribution function $\rho(r)$ of parallel LC molecules for a LC monolayer confined by (a) the (100) surfaces, (b) the (110) surfaces, and (c) the (111) surfaces.

$xy$ plane, thus $r = \sqrt{(X_i - X_j)^2 + (Y_i - Y_j)^2}$, where $(X_i, Y_i)$ is the plane center of mass of LC molecule $i$. For the (100) surface, the driving velocity dependence of $\rho(r)$ is reported in Fig. 12(a). For $V = 0.01$, $V = 0.05$, and $V = 0.1$, the distribution functions have roughly the same profiles, with the values of each peak decreasing with increasing driving velocity. Only one peak can be observed for $V = 0.5$, and its height is much smaller than that for lower velocities, implying that it is more difficult to find two LC molecules pointing in the same direction. The LCs align themselves according to the surface mesh at low velocity, but get disordered at high velocity. Figure 12(b) shows $\rho(r)$ for the system confined by (110) surfaces: We observe multiple peaks at all considered driving velocities. The height of the peaks is roughly fixed at large distances because the LC film possesses long-range order (consistent with snapshots of the system; see Fig. 7). At a low driving velocity, $V = 0.01$, the height of the first peak is much larger than those of the larger driving velocities, which again implies that the film gets more disordered at higher sliding velocities. Similar trends in the driving velocity dependence of the pair distribution function for the (111) surface can also be observed from the data reported in Fig. 12(c).

## IV. CONCLUSIONS

In summary, our findings reveal that the friction force in the boundary lubrication of a LC monolayer can be controlled by the imposed shear velocity, and is intimately related to the atomic scale structure of the confining surfaces. For all three kinds of surfaces considered, (100), (110), and (111), regular stick-slip events (with some details depending on the surface structure, e.g., the presence or absence of damped oscillations of the bottom plate) are observed clearly for low shear velocities, and all of the molecules of the LC film strongly interact with the confining surfaces. Thus the LC molecules orient to align with the surface crystal structure and have been found to exhibit "order-disorder" transitions when moving from the stick to the slip state (and vice versa): Our results show that the LC molecules exhibit significant orientational order in the stick state, but get less ordered (in a manner or to the extent that depends on the details of the structure of the confining surfaces) when the bottom plate slips.

Besides the surface mesh, the direction and magnitude of the shear flow are important parameters determining the frictional properties of the LC monolayer lubricant. In general, the effect of the shear flow competes with the influence of the surface-induced orientation. While in the limit of a very small sliding velocity, the surface structure controls the preferred orientation of the LC molecules; for somewhat higher, "intermediate" velocities, the LC molecules do not have enough time to rearrange according to the surface-induced preferred orientation between two slip events and, consequently, the time dependence of the friction force exhibits irregular or "chaotic" stick-slip dynamics. For even higher driving velocities, the LCs become preferentially aligned in the direction of the shear flow, and the system enters a smooth sliding state with the maximum friction force much smaller than that of the low-velocity stick-slip phase.

Here we have considered a simplified (or "coarse-grained") model system of elongated molecules confined by surfaces of different structures, in order to gain insight into the general mechanisms related to frictional properties of systems such as LC-lubricated friction. Some final remarks are in order: First, one should extend the present study to consider MD

simulations of full atomistic models of real LC molecules (5CB, 6CB, etc.), confined by real atomistic surfaces. We expect the insights of the present study to be useful for such future extensions. Such studies could also consider the effects of disorder, surface mismatch, or surface misalignment, all of which are known to have important consequences for friction [47]. The same applies to considering a thicker lubricant film, where the effects due to the structure of the confining surfaces could be less pronounced. Finally, we have demonstrated here that the frictional properties of the system depend on things such as the structure of the confining surfaces and the imposed shear rate. However, LC lubricants exhibit an additional promising possibility, i.e., their orientational order is known to be tunable by applying external fields [5]. Given that the frictional properties of the LC system have been shown to be connected to their ordering characteristics [15], exploring the possibility of friction control of LC lubricants via external fields should be worth future investigations.

## ACKNOWLEDGMENTS

We are grateful to the financial support by the Academy of Finland through the Centres of Excellence Program (Project No. 251748) and via an Academy Research Fellowship (L.L., Project No. 268302). We are also grateful to the COST Action No. MP1303. The calculations presented above were performed using computer resources within the Aalto University School of Science "Science-IT" project. We also acknowledge the computational resources provided by CSC (Finland).

[1] B. Bhushan, J. N. Israelachvili, and U. Landman, Nature (London) **374**, 607 (1995).
[2] C. H. Scholz, Nature (London) **391**, 37 (1998).
[3] B. J. Hamrock, S. R. Schmid, and B. O. Jacobson, *Fundamentals of Fluid Film Lubrication* (CRC, Boca Raton, FL, 2004), Vol. 169.
[4] J. Krim, Adv. Phys. **61**, 155 (2012).
[5] J. Prost, *The Physics of Liquid Crystals* (Oxford University Press, New York, 1995), Vol. 83.
[6] T. E. Fischera, S. Bhattacharyaa, R. Salhera, J. L. Lauerb, and Y. J. Ahnb, Tribol. Trans. **31**, 442 (1988).
[7] R. J. Bushby and K. Kawata, Liq. Cryst. **38**, 1415 (2011).
[8] T. Amann and A. Kailer, Wear **271**, 1701 (2011).
[9] T. Amann and A. Kailer, Tribol. Lett. **41**, 121 (2011).
[10] T. Amann and A. Kailer, Tribol. Lett. **37**, 343 (2010).
[11] F. J. Carrión, G. M. Nicolás, P. Iglesias, J. Sanes, and M. D. Bermúdez, Int. J. Mol. Sci. **10**, 4102 (2009).
[12] L. Noirez, G. Pepy, and P. Baroni, J. Phys.: Condens. Matter **17**, S3155 (2005).
[13] C. Pujolle-Robic and L. Noirez, Phys. Rev. E **68**, 061706 (2003).
[14] S. H. J. Idziak, C. R. Safinya, R. S. Hill, K. E. Kraiser, M. Ruths, E. Warriner, S. Steinberg, K. S. Liang, and J. N. Israelachvili, Science **264**, 1915 (1994).
[15] C. Cheng, L. Kellogg, S. Shkoller, and D. Turcotte, Proc. Natl. Acad. Sci. **105**, 7930 (2007).
[16] A. Artsyukhovich, L. D. Broekman, and M. Salmeron, Langmuir **15**, 2217 (1999).
[17] D. Gourdon and J. N. Israelachvili, Phys. Rev. E **68**, 021602 (2003).
[18] M. R. Wilson, Int. Rev. Phys. Chem. **24**, 421 (2005).
[19] S. Sarman and D. J. Evans, J. Chem. Phys. **99**, 9021 (1993).
[20] S. Sarman, J. Chem. Phys. **103**, 10378 (1995).
[21] S. Sarman and A. Laaksonen, J. Chem. Phys. **131**, 144904 (2009).
[22] S. Sarman, J. Chem. Phys. **108**, 7909 (1998).
[23] A. M. Smondyrev, G. B. Loriot, and R. A. Pelcovits, Phys. Rev. Lett. **75**, 2340 (1995).
[24] G. Cinacchi, L. D. Gaetani, and A. Tani, J. Chem. Phys. **122**, 184513 (2005).
[25] J. G. Gay and B. J. Berne, J. Chem. Phys. **74**, 3316 (1981).
[26] J. Karjalainen, J. Lintuvuori, V. V. Telkki, P. Lantto, and J. Vaara, Phys. Chem. Chem. Phys. **15**, 14047 (2013).
[27] P. Tian, D. Bedrov, G. D. Smith, and M. Glaser, J. Chem. Phys. **115**, 9055 (2001).
[28] P. Tian, D. Bedrov, G. D. Smith, M. Glaser, and J. E. Maclennan, J. Chem. Phys. **117**, 9452 (2002).
[29] P. Tian and G. D. Smith, J. Chem. Phys. **116**, 9957 (2002).
[30] J. Zhang, J. S. Hansen, B. D. Todd, and P. J. Daivis, J. Chem. Phys. **126**, 144907 (2007).
[31] N. V. Priezjev, J. Chem. Phys. **136**, 224702 (2012).
[32] C. Drummond and J. Israelachvili, Macromolecules **33**, 4910 (2000).
[33] C. Drummond and J. Israelachvili, Phys. Rev. E **63**, 041506 (2001).
[34] I. S. Aranson, L. S. Tsimring, and V. M. Vinokur, Phys. Rev. B **65**, 125402 (2002).
[35] D. Frenkel and B. Smit, *Understanding Molecular Simulation: From Algorithms to Applications*, 2nd ed. (Academic, New York, 2001).
[36] D. J. Evans and G. P. Morriss, *Statistical Mechanics of Nonequilibrium Liquids* (Academic, London, 1990).
[37] P. A. Thompson and M. O. Robbins, Phys. Rev. A **41**, 6830 (1990).
[38] P. A. Thompson and S. M. Troian, Nature (London) **389**, 360 (1997).
[39] T. F. Miller, M. Eleftheriou, P. Pattnaik, A. Ndirango, D. Newns, and G. J. Martyna, J. Chem. Phys. **116**, 8649 (2002).
[40] S. Plimpton, J. Comp. Phys. **117**, 1 (1995).
[41] D. C. Rapaport, *The Art of Molecular Dynamics Simulation*, 2nd ed. (Cambridge University Press, Cambridge, 2004).
[42] J. Gao, W. D. Luedtke, and U. Landman, J. Phys. Chem. B **102**, 5033 (1998).
[43] P. A. Thompson and M. O. Robbins, Science **250**, 792 (1990).
[44] W. Humphrey, A. Dalke, and K. Schulten, J. Molec. Graphics **14**, 33 (1996).
[45] See Supplemental Material at http://link.aps.org/supplemental/10.1103/PhysRevE.90.012404 for a video file of instantaneous configurations of the LC film.
[46] J. Gao, W. Luedtke, and U. Landman, J. Chem. Phys. **106**, 4309 (1997).
[47] A. Jabbarzadeh, P. Harrowell, and R. Tanner, Tribol. Int. **40**, 1574 (2007).